JOURNAL OF MATERIALS SCIENCE 28 (1993) 5793–5799

Fabrication of zirconia–alumina functionally gradient material by superplastic diffusion bonding

TAKAYUKI NAGANO
Research and Development Center, Hamamatsu Development Division, Suzuki Motor Corporation, Takatsuka-cho, Hamamatsu 432-91, Japan

FUMIHIRO WAKAI
Ceramic Science Department, Government Industrial Research Institute Nagoya, Hirate-cho 1-1, Kita-ku, Nagoya 462, Japan

Functionally gradient ZrO_2–Al_2O_3 material was fabricated by superplastic diffusion bonding in the present study. Conditions included a bonding temperature of 1550 °C, a time of 30 min, and strains of 17, 33 and 50%. Complete bonding was obtained under all of these bonding conditions. The apparent bending strength of functionally gradient material fabricated by superplastic diffusion bonding was 1860 MPa at the strain of 50%.

1. Introduction

Recent advances in technology require structural materials that can be used in severe environments. Composite materials have been developed to overcome the performance limitations of monolithic materials. Further development of materials design has led to the concept of functionally gradient materials (FGM), in which the composition and concentration of the dispersed phase are elaborately distributed. These FGM have been fabricated by chemical vapour deposition (CVD) [1, 2], chemical vapour infiltration (CVI) [3], physical vapour deposition (PVD) [4], thin sheet lamination [5], plasma spray coating [6, 7], self propagating high temperature synthesis [8], and gas-pressure combustion sintering [9]. The present authors systematically investigated diffusion bonding between superplastic ceramics with different thermal expansion coefficients. We demonstrated that complete bonding of ZrO_2/Al_2O_3 composites with various Al_2O_3 contents could be achieved under appropriate conditions [10, 11].

This bonding technique will make it possible to fabricate FGM from stacked, thin sheets of fine-grained ceramics and/or metals by means of diffusion bonding, so that the composition of the material changes either continuously or stepwise. With this manufacturing method, large and complex-shaped FGM components can be fabricated at lower than usual cost, because superplastic forming and diffusion bonding (SPF/DB) can be performed at the same time. Accordingly, in the present study, we fabricated ZrO_2–Al_2O_3 FGM by using superplastic diffusion bonding, and we then investigated the bonding and mechanical properties of FGM.

2. Experimental procedure

The materials used in the bonding tests were Y_2O_3 stabilized tetragonal ZrO_2 polycrystals (Y-TZP) (ZYS, Tosoh Co., Tokyo, Japan), ZrO_2/Al_2O_3 composites (super-Z, Tosoh Co.) [X $ZrO_2/(100 - X)$ Al_2O_3, in wt %, where X = 80, 60, 40, 20], and Al_2O_3 (A-392, Narumi China Co., Nagoya, Japan). Y-TZP was sintered at 1550 °C for 1 h in air. The composite powder of ZrO_2/Al_2O_3 was first die pressed, then cold isostatically pressed at 300 MPa. The compacts were sintered at 1400–1450 °C in air and hot isostatically pressed at 100 MPa and 1500 °C for 30 min in argon. The ZrO_2 contained 3 mol % Y_2O_3 in a solid solution [12, 13]. Al_2O_3 was commercially available. Some properties of the materials are summarized in Table I. Mechanical properties were experimental values. Sample density was measured by Archimedes method. The bending strength was evaluated by the three-point bending test (lower span = 30 mm). The average grain size is defined by a linear intercept length as follows:

$$d_{av} = 1.776L \quad (1)$$

where d_{av} is average grain size and L is the linear intercept length. Young's modulus was measured by the ultrasonic pulse method. The superplasticity of Y-TZP [14] and of the ZrO_2/Al_2O_3 composite [15, 16] was confirmed in tension tests at elevated temperatures. The as-obtained ceramic bodies were cut, using a diamond cutter, and ground with a no. 200 diamond wheel; the bonding surfaces were finished with a no. 400 diamond wheel. The specimens measured 15 × 40 × 1 mm, with a bonding surface roughness of $R_{max} < 3$ μm. The bonding method is schematically illustrated in Fig. 1. Bonding was performed using a universal testing machine with a furnace at 1550 °C in air. The plastic deformation resistance in materials increased with Al_2O_3 content [16]. The difference in deformation resistance among materials decreased

0022–2461

TABLE I Some properties of materials

Material	ZrO_2 (wt %)	Al_2O_3 (wt %)	Density ($g\,cm^{-3}$)	Bending strength (MPa)	Grain size (μm)	Young's modulus (GPa)	Shear modulus (GPa)	Thermal expansion ($1/°C(\times 10^{-6})$)
Y-TZP	99.7		6.05	750	0.59	200	76	12.0
3*Y*20*A*	79.9	20.0	5.50	2300	0.77	250	97	11.2
3*Y*40*A*	59.9	40.0	5.10	2300	0.79	300	119	10.4
3*Y*60*A*	39.9	60.0	4.60	2000	0.80	335	134	9.94
3*Y*80*A*	19.9	80.0	4.30	1200	1.06	370	150	9.48
Al_2O_3		92.0	3.53	360	4.77	280	113	8.71

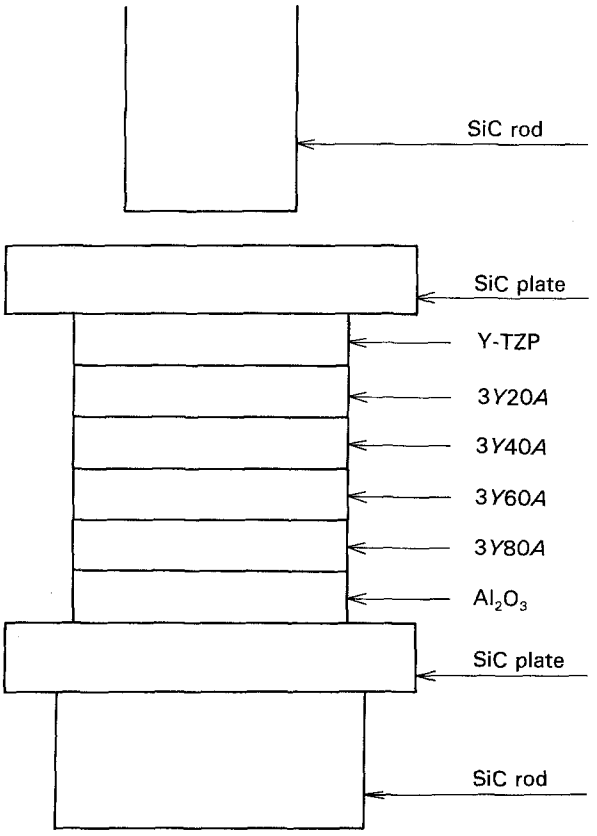

Figure 1 Illustration of bonding set.

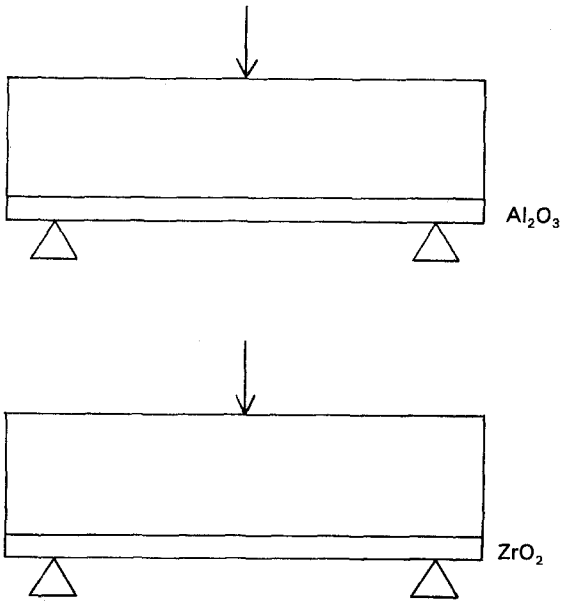

Figure 2 Illustration of bending test of FGM.

with increasing temperature. Therefore, we chose a bonding temperature of 1550 °C so as to minimize the difference in deformation resistance among materials and considering the heat resistance of the SiC jig. The specimens were heated and compressed by a SiC jig at a crosshead speed of 0.01 mm min^{-1}. After the specimens had been deformed to a fixed strain point (17, 33, 50 %), the crosshead was stopped and held for 30 min. The specimens were cooled in the furnace. A diamond cutter was used to slice the bonded materials into rectangular bars, and the specimens were ground with no. 200 and no. 400 diamond wheels. The bend specimens were $3 \times 4 \times 40$ mm. Bending strength was measured at room temperature by the three-point bending test (lower span = 30 mm) at a crosshead speed of 0.5 mm min^{-1} in two ways; the tensile stress was applied on either the Y-TZP side or the Al_2O_3 side. An illustration of the bending test is shown in Fig. 2.

3. Results

A photograph of the ZrO_2–Al_2O_3 FGM fabricated by superplastic diffusion bonding is shown in Fig. 3. A slight warp was observed in the ZrO_2–Al_2O_3 FGM fabricated by superplastic diffusion bonding, as illustrated in Fig. 4(a). The degree of warp in Fig. 4 is exaggerated for visual clarity. The deflection at the centre was 132 μm for a specimen which was compressed to a strain of 17 %. The degree of warp increased with strain. The FGM was warped by the residual tensile stress produced at the ZrO_2-rich layers when the FGM, which consisted of several layers with different thermal expansion coefficients, cooled from the bonding temperature of 1550 °C to ambient temperature. Apparently, the final residual stress in each layer of FGM was relaxed by some plastic deformation. The surfaces of the bending specimens cut from the bonding body were ground, so that the thickness of the Y-TZP and Al_2O_3 layers decreased, as shown in Fig. 4(b).

Scanning electron micrographs of the bonding interface of the ZrO_2–Al_2O_3 FGM that were deformed to a strain of 17% are shown in Fig. 5. All of the bonding interfaces, except that of the 3*Y*80*A*–Al_2O_3 completely bonded with the aid of superplastic deformation. At strains of 33% and 50%, all interfaces except that of the 3*Y*80*A*–Al_2O_3 completely bonded,

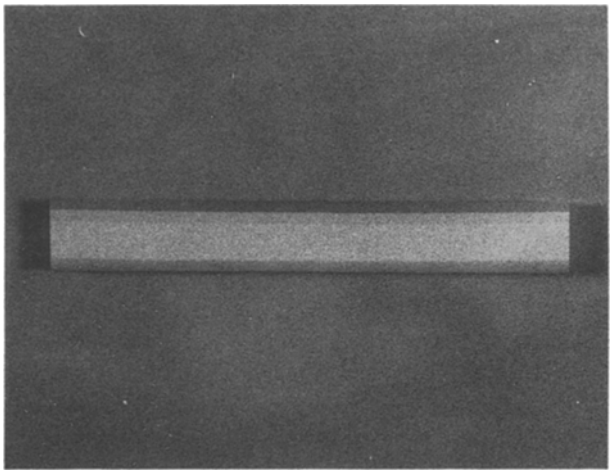

Figure 3 Photograph of ZrO_2–Al_2O_3 FGM fabricated by superplastic diffusion bonding.

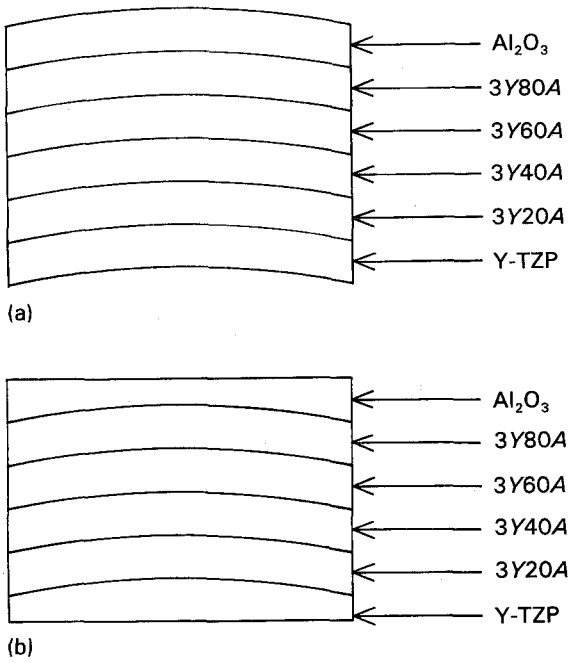

Figure 4 Schematic figure of FGM. (a) before grinding; (b) after grinding.

too. Under present experiment conditions, complete bonding of the 3*Y*80*A*–Al_2O_3 interface was difficult, because the Al_2O_3 grain sizes were too large and plastic deformation resistance was high.

The relationship between the apparent bending strength of the FGM and the applied strain during the bonding procedure is shown in Fig. 6. The apparent bending strength of the FGM in Fig. 6 was calculated using the following equation, assuming that the bending stress is applied on a uniform elastic beam:

$$\sigma = 3P_fL/2bd^2 \quad (2)$$

where σ represents bending strength, P_f the applied load, L the span, b the width of the specimen, and d the specimen height. The apparent bending strength of ZrO_2–Al_2O_3 FGM deformed at a strain of 17% was 375 MPa when tensile stress was applied on the Al_2O_3 side and 1340 MPa when tensile stress was applied on the Y-TZP side. These apparent bending strengths were higher than the strengths of the base materials (360 MPa for Al_2O_3 and 750 MPa for ZrO_2).

4. Discussion

The apparent bending strength of ZrO_2–Al_2O_3 FGM measured by applying tensile stress on the ZrO_2 side was 1.79 times as high as the strength of the ZrO_2 base material. To analyse this result, we used the finite element method (FEM) to calculate the stress distribution of ZrO_2–Al_2O_3 FGM that had been deformed up to 17% during bonding. We then analysed the fabrication of the FGM, the preparation of the bend specimens, and the bending test itself.

The simulation began with ZrO_2–Al_2O_3 FGM that had just bonded by deformation at elevated temperature before the start of cooling. We determined the dimensions of the FEM model by calculating the thickness of each layer at elevated temperature (before thermal contraction) from the measured thickness of each layer of as-fabricated FGM. The width of the FEM model was set at 4 mm: actually, the as-fabricated FGM had a width of 15 mm, and the bonded body was cut into 4 mm wide rectangular bend specimens. Preliminary calculations had indicated that specimen width did not affect the residual stress induced by thermal contraction, so we adopted 4 mm instead of 15 mm for the width of the FEM model. Because the specimen was symmetrical, only one-fourth of it was modelled, as shown in Fig. 7. Translation perpendicular to the symmetry plane was constrained in the 3-dimensional finite-element mesh model. The size of the element mesh varied, with smaller elements near the bonding interfaces, the load points of three-point bending and the roller, where the largest stress gradient was expected. The surface of as-fabricated FGM which maintained its residual stress after thermal contraction was ground to prepare bend specimens. In the present model, the thickness of the mesh in the Al_2O_3 or Y-TZP surface layer was determined so that the grinding could be simulated by removing the corresponding elements. The following conditions were set as a premise for calculation. During cooling to 20 °C from the bonding temperature of 1550 °C, the plastic deformation and the temperature dependence of physical properties in the materials were not considered. When the bend specimen was prepared by grinding, the residual stress of centre was estimated accurately by removing from the surface elements corresponding to the thickness of the grinding margin at the centre. The influence of curvature on the surface, however, was not considered in the present case. Furthermore, we calculated the stress distribution of the ZrO_2–Al_2O_3 FGM under an average fracture load (P_f in Equation 2) in a three-point bending test. The degree of freedom in the loading direction at the contact points of the lower span was thus constrained.

Deflection of the ZrO_2–Al_2O_3 FGM induced by thermal contraction during fabrication is shown in Fig. 8. The calculated deflection curve was similar to the measured deflection curve, but the calculated value was approximately 20% higher than the meas-

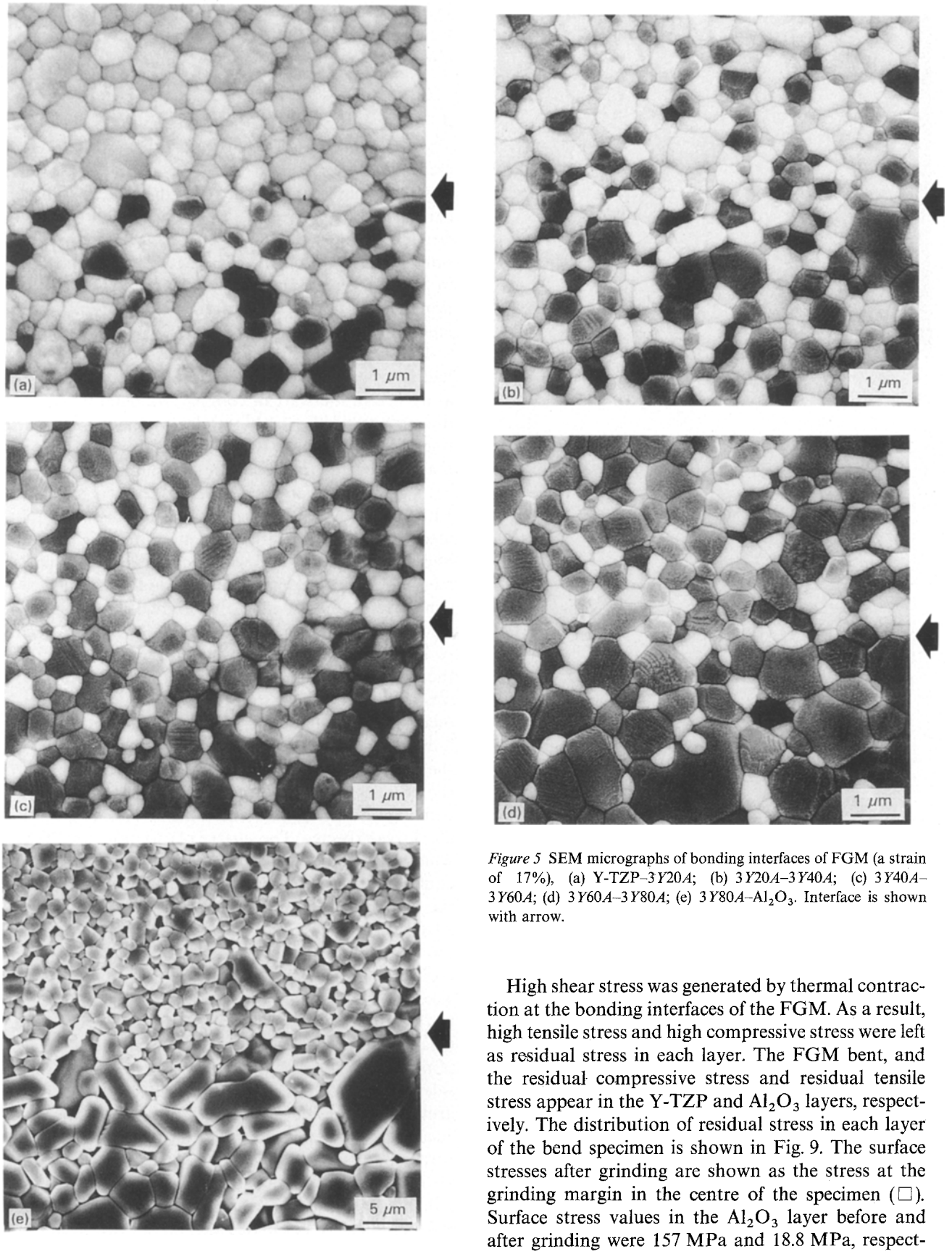

Figure 5 SEM micrographs of bonding interfaces of FGM (a strain of 17%), (a) Y-TZP–3*Y*20*A*; (b) 3*Y*20*A*–3*Y*40*A*; (c) 3*Y*40*A*–3*Y*60*A*; (d) 3*Y*60*A*–3*Y*80*A*; (e) 3*Y*80*A*–Al_2O_3. Interface is shown with arrow.

ured value. The discrepancy between the deflections may be attributable to the fact that the bonding interface is fixed in the FEM model, so that microscopic sliding deformation at the bonding interface during the actual bonding process is not considered in that model.

High shear stress was generated by thermal contraction at the bonding interfaces of the FGM. As a result, high tensile stress and high compressive stress were left as residual stress in each layer. The FGM bent, and the residual compressive stress and residual tensile stress appear in the Y-TZP and Al_2O_3 layers, respectively. The distribution of residual stress in each layer of the bend specimen is shown in Fig. 9. The surface stresses after grinding are shown as the stress at the grinding margin in the centre of the specimen (□). Surface stress values in the Al_2O_3 layer before and after grinding were 157 MPa and 18.8 MPa, respectively. The difference in stress value was large because the grinding margin was thick in the Al_2O_3 layer. In the Y-TZP layer, however, the grinding margin was thin, and the difference in stress was small. In the present analysis, residual stress after grinding, at the centre of the specimen, was calculated by removing the elements corresponding to the grinding margin. The slight error in the calculated residual stress may have occurred because we ignored the redistribution of

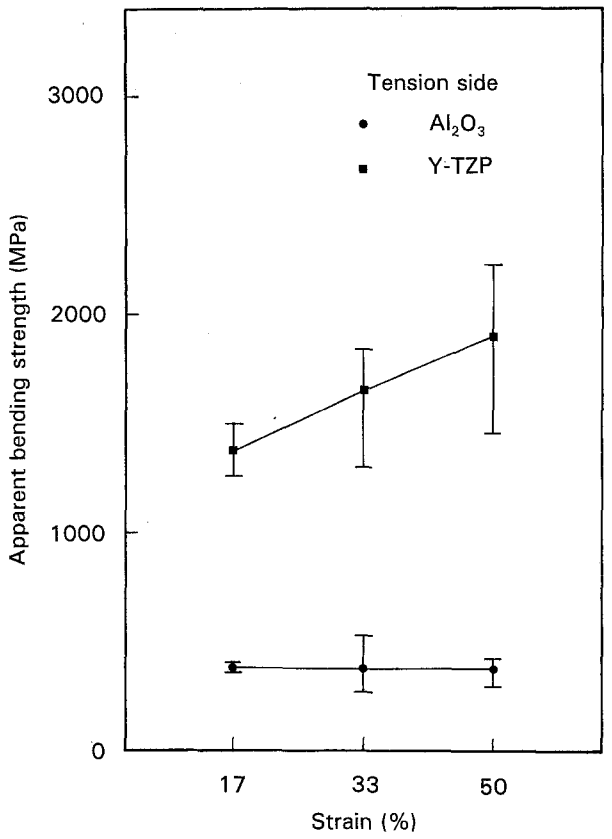

Figure 6 Relationship between apparent bending strength and strain in bonding.

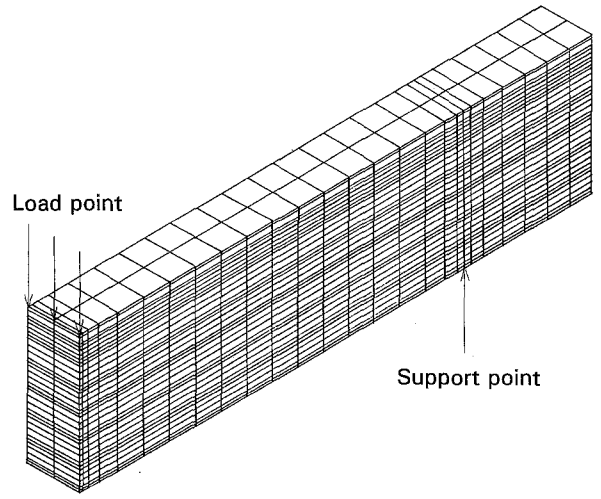

Figure 7 FEM model for bend specimen of FGM.

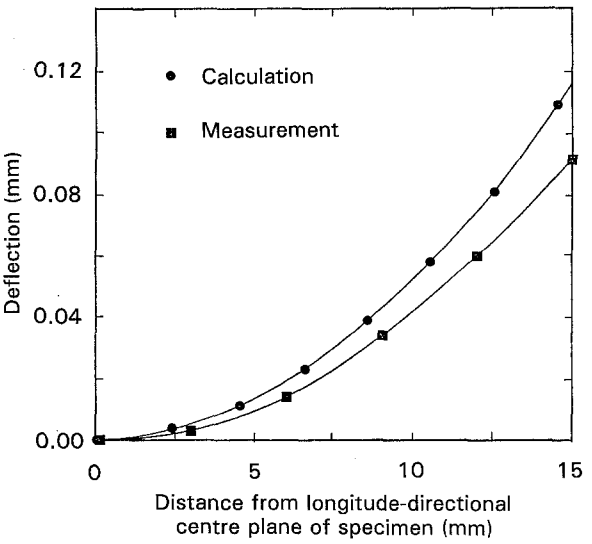

Figure 8 Deflection of FGM by thermal contraction.

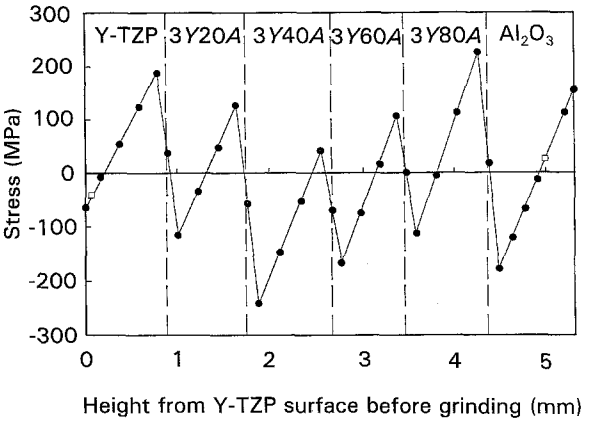

Figure 9 Residual stress in each layer of FGM (□ after grinding; • tensile stress; – compressive stress).

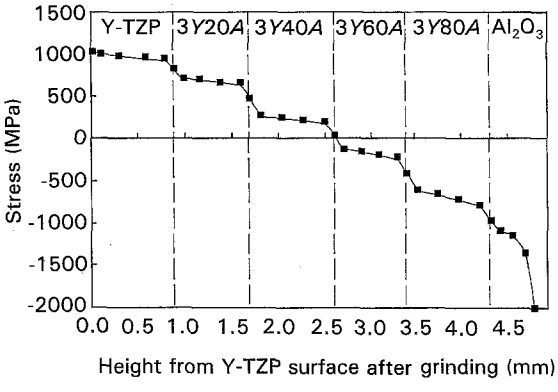

Figure 10 Stress distribution when Y-TZP is the tension side.

residual stress caused by the shift of the neutral plane in the Y-TZP and Al_2O_3 layers, the effect of external force during grinding, and the effects of plastic deformation during cooling.

The stress distribution of FGM in the three-point bending test was calculated by the FEM, incorporating the residual stress. The stress distribution when a tensile stress is applied to the Y-TZP layer is shown in Fig. 10 and that when tensile stress is applied to the Al_2O_3 layer is shown in Fig. 11. These stress distributions were calculated by assuming that the fracture load (P_f in Equation 2) had been applied to the bend specimens. Table II summarizes the apparent bending strength ($\sigma_{FGM}^{apparent}$) calculated using Equation 2, from the fracture load (P_f) in the three-point bending test of FGM, and the surface stress ($\sigma_{FGM}^{surface}$), calculated from the FEM analysis. The subscript (Al_2O_3, Y-TZP) indicates the layer at the tension side of the FGM. Table III summarizes the ratio of apparent bending strength of the FGM to the bending strength of the base material ($\sigma_{Y\text{-}TZP}$ or $\sigma_{Al_2O_3}$) and the ratio of the apparent bending strength of the FGM ($\sigma_{FGM}^{apparent}$) to the calculated surface stress ($\sigma_{FGM}^{surface}$). Here, the subscripts Al_2O_3 and Y-TZP are the bending strengths of

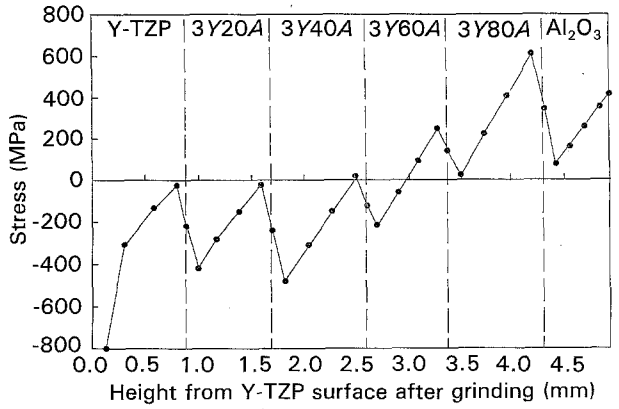

Figure 11 Stress distribution when Al_2O_3 is the tension side.

TABLE II Apparent bending strength and surface stress in three-point bending test

	$\sigma^{apparent}_{FGM(Al_2O_3)}$	$\sigma^{surface}_{FGM(Al_2O_3)}$
Tension side Al_2O_3	375	420
	$\sigma^{apparent}_{FGM(Y\text{-}TZP)}$	$\sigma^{surface}_{FGM(Y\text{-}TZP)}$
Tension side Y-TZP	1341	1018

TABLE III Ratio of apparent bending strength to base material strength, and ratio of apparent bending strength to surface stress

$\sigma^{apparent}_{FGM(Al_2O_3)}/\sigma_{(Al_2O_3)}$	$\sigma^{apparent}_{FGM(Al_2O_3)}/\sigma^{surface}_{(Al_2O_3)}$
1.04	0.89
$\sigma^{apparent}_{FGM(Y\text{-}TZP)}/\sigma_{(Y\text{-}TZP)}$	$\sigma^{apparent}_{FGM(Y\text{-}TZP)}/\sigma^{surface}_{(Y\text{-}TZP)}$
1.79	1.32

the base materials (Al_2O_3 and Y-TZP). First, when tensile stress was applied to the Y-TZP side, the apparent bending strength of the FGM increased remarkably, to 1.79 times higher than the strength of Y-TZP. Results of FEM analysis, however, showed that the strength of the Y-TZP surface layer of the FGM increased to only 1.32 times the strength of Y-TZP. This FGM was fabricated by applying a large compressive deformation. As is well known from the results of hot pressing [12, 13] and sinter forging [17, 18], the strength of a material with fine grains increases when compressive stress is applied at elevated temperature [11, 19]. The increase in strength is attributed to shrinkage and elimination of large pores of defects during compressive superplastic deformation. Therefore, when tensile stress is applied to the Y-TZP side of the bend specimen, the strengthening of FGM with increasing strain in Fig. 6 was caused by the strengthening of the Y-TZP layer by superplastic deformation. On the other hand, when tensile stress was applied to the Al_2O_3 side of the bend specimen, the FEM analysis showed that the strength of the Al_2O_3 layer in the FGM decreased to 0.9 times the strength of Al_2O_3. The strength of the FGM did not increase with increasing strain, as shown in Fig. 6. Because large-grained Al_2O_3 deformed very little, even though the FGM could be deformed as a whole, overall strengthening was not achieved. If, therefore, FGM is fabricated using fine-grained Al_2O_3 and has superior plastic deformation characteristics at elevated temperatures, the strength of the Al_2O_3 layer should be improved and the strength of the FGM increase further. The bending strength of the FGM increased with increasing strain when the Y-TZP side was the tension side in Fig. 6. The phenomenon was caused by increasing residual compressive stress in the Y-TZP surface with increasing warp of the FGM and increasing strength of the base material with increasing strain in compressive deformation.

5. Conclusion

ZrO_2–Al_2O_3 FGM was fabricated by superplastic diffusion bonding at a bonding temperature of 1550 °C and at strains of 17, 33 and 50%. Residual stress and stress distribution in the bend specimen were evaluated by FEM. The results of the present study are summarized as follows.

1. The interface bonded completely by superplastic deformation, and ZrO_2–Al_2O_3 FGM was fabricated successfully.
2. The apparent bending strength of the ZrO_2–Al_2O_3 FGM was significantly different according to the direction of applied stress. When the tension side was the Y-TZP, the apparent bending strength of the specimen (strain of 50%) was 1860 MPa; when the tension side was Al_2O_3, the apparent bending strength (strain of 50%) was 330 MPa.
3. The stress analysis by FEM qualitatively agreed with the results for the ZrO_2–Al_2O_3 FGM from the bending test.

Acknowledgement

We would like to thank T. Sasahara for helpful work.

References

1. M. SASAKI and T. HIRAI, in Proceedings of the First International Symposium on Functionally Gradient Materials, edited by M. Yamanouchi, M. Koizumi, T. Hirai and I. Shiota, (Functionally Gradient Materials Forum, Tokyo, 1990) p. 83.
2. M. SASAKI, H. SUZUKI and T. HIRAI, *ibid.*, p. 231.
3. R. NASLAIN, *ibid.*, p. 71.
4. K. FRITSCHER and W. BUNK, *ibid.*, p. 91.
5. M. TAKEMURA, A. YOSHITAKE, H. HAYAKAWA, T. HYAKUBU and M. TAMURA, *ibid.*, p. 97.
6. H. STEFFENS, M. DVORAK and M. WEWEL, *ibid.*, p. 139.
7. T. FUKUSHIMA, S. KURODA and S. KITAHARA, *ibid.*, p. 145.
8. N. YANAGISAWA, N. SATA and N. SANADA, *ibid.*, p. 179.
9. Y. MIYAMOTO, H. NAKANISHI, I. TANAKA, T. OKAMOTO and O. YAMADA, *ibid.*, p. 257.
10. T. NAGANO, H. KATO and F. WAKAI, in Proceedings of International Meeting on Advanced Materials, Vol. 7, Superplasticity, edited by M. Kobayashi and F. Wakai, (Materials Research Society, Pittsburgh, 1989) p. 285.
11. T. NAGANO, H. KATO and F. WAKAI, *J. Amer. Ceram. Soc.* **73** (1990) 3476.
12. K. TSUKUMA, K. UEDA and M. SHIMADA, *ibid.* **68** (1985) C-4.
13. *idem.*, *ibid.* **68** (1985) C-56.

14. F. WAKAI, S. SAKAGUCHI and Y. MATSUNO, *Adv. Ceram. Mater.* **1** (1986) 259.
15. F. WAKAI and H. KATO, *ibid.* **3** (1988) 71.
16. F. WAKAI, Y. KODAMA, S. SAKAGUCHI, N. MURAYAMA, H. KATO and T. NAGANO, in Proceedings of MRS International Meeting on Advanced Materials, Vol. 7, Superplasticity, edited by M. Kobayashi and F. Wakai, (Materials Research Society, Pittsburgh, 1989) p. 259.
17. P. C. PANDA, J. W. WANG and R. RAJ, *J. Amer. Ceram. Soc.* **71** (1988) C507.
18. M. YAMANA, Y. YAMAMOTO, S. NAKAMURA, K. KITAGAWA, T. YOSHIMURA, T. MANO and Y. SHINTANI, *J. Ceram. Soc. Jpn* **97** (1989) 758.
19. T. NAGANO, H. KATO and F. WAKAI, *J. Mater. Sci.* **26** (1991) 4985.

Received 15 June 1992
and accepted 4 January 1993